Appl Nanosci (2013) 3:109–117
DOI 10.1007/s13204-012-0090-z

ORIGINAL ARTICLE

Analysis of temperature and wave function penetration effects in nanoscale double-gate MOSFETs

E. Farzana · S. Chowdhury · R. Ahmed · M. Ziaur Rahman Khan

Received: 15 December 2011 / Accepted: 2 March 2012 / Published online: 30 March 2012

Abstract Wave function penetration has significant impact on nanoscale devices having ultrathin gate oxide. Although wave function penetration effects on ballistic drain current and capacitance-voltage characteristics in nanoscale devices have been reported in literature, to the best of the authors' knowledge, effects of temperature on drain current incorporating with and without wave function penetration are yet to be studied. In this work, the impacts of temperature, gate dielectric and film thickness in wave function penetration on ballistic drain current of nanoscale double-gate (DG) MOSFETs are presented. The effects are observed using two-dimensional self-consistent solution of Schrödinger and Poisson equations. It has been obtained that temperature effect on drain current is greatly dependent on silicon surface orientation. Drain current of DG MOSFETs fabricated on ⟨110⟩ surface is more sensitive to temperature compared to ⟨001⟩ surface. This has been obtained for both the cases with and without incorporating wave function penetration in silicon–gate oxide interface. Electrostatics behind this phenomenon has been explained from the transmission probability of electrons from source to drain which is largely influenced by temperature on ⟨110⟩ surface compared to ⟨001⟩. Moreover, the transmission coefficient is significantly affected by wave function penetration in ⟨110⟩ than ⟨001⟩ surface. Both these demonstrate greater sensitivity of temperature and wave function penetration in ⟨110⟩ silicon surface orientation compared to ⟨001⟩. Furthermore, gate dielectric with lower conduction band offset and device scaling with thin channel thickness tend to exhibit greater impact of wave function penetration.

Keywords Wave function penetration · Surface orientation · Ballistic drain current · Transmission coefficient

E. Farzana (✉) · S. Chowdhury · R. Ahmed · M. Z. R. Khan
Department of Electrical and Electronic Engineering,
Bangladesh University of Engineering and Technology,
Dhaka 1000, Bangladesh
e-mail: Li.eee05@gmail.com

S. Chowdhury
e-mail: SChowdhury.eee@gmail.com

R. Ahmed
e-mail: rar.eee05@gmail.com

M. Z. R. Khan
e-mail: zrkhan@eee.buet.ac.bd

Introduction

Double-gate (DG) MOSFET is one of the promising solutions of upcoming modified device structures since it performs more efficiently compared to its single-gate (SG) bulk counterpart (Iwai 2009; S.I. Association 2009). DG MOSFETs have better control over short channel effects (SCE), threshold voltage roll-off, drain induced barrier lowering (DIBL) and reduced subthreshold swing than SG MOSFETs (Farzana et al. 2012; Ashraf et al. 2009). With decrease in device dimensions, certain quantum mechanical effects modify device characteristics significantly. In the quantum mechanical simulation schemes of DG MOSFETs, the boundary condition commonly used to solve the Schrödinger's equation is that wave functions go to zero at the silicon–gate oxide interface. This is consistent if an infinite potential barrier height for inversion layer carriers at the silicon–gate oxide interface is assumed. However, since the actual barrier height is finite and nearly a few electron-volts, wave function actually penetrates into the gate oxide. While this penetration has negligible effects in devices with thick oxide layers, its neglect in nanoscale

MOSFETs with thin gate oxide cannot be justified. The importance of incorporating wave function penetration in modeling nanoscale MOSFETs has been investigated in literature (Ashraf et al. 2009; Haque and Kauser 2003; Kauser et al. 2002; Chim et al. 2003; Yunus and Haque 2003). The effects of wave function penetration into the gate oxide on gate capacitance of nanoscale p-MOS devices have been reported in (Haque and Kauser 2003). In (Kauser et al. 2002), the penetration effects on properties of inversion layers and device dimensions have been studied. A comparison of wave function penetration effects on ballistic drain current in bulk MOSFETs fabricated on $\langle 100 \rangle$ or $\langle 111 \rangle$ silicon surfaces has been demonstrated in (Yunus and Haque 2003) for bulk MOSFETs. The wave function penetration effect and charge quantization effects on capacitance voltage characteristics have been investigated in (Chim et al. 2003). These results, although insightful, are explored with 1D Schrödinger-Poisson solver that cannot capture the lateral effect of source to drain tunneling accurately. Later, the modification of ballistic drain current due to wave function penetration and its sensitivity to scaling of device have been explored in (Ashraf et al. 2009) in different crystal orientations of silicon wafer using 2D quantum ballistic transport model (Ren et al. 1914; Venugopal et al. 2002). However, effects of temperature and wave function penetration simultaneously are yet to be reported in literature.

In this work, wave function penetration along with temperature changing effects are heuristically analyzed using nanoMOS 3.5 (nanoHUB http://www.nanohub.org). This depicts the influence of temperature for both crystal surface ($\langle 001 \rangle$ and $\langle 110 \rangle$).$\langle 110 \rangle$ surface is important for realizing higher speed scaled complementary MOS (CMOS) circuits for having high hole mobility (Tsutsui and Hiramoto 2006). It has been obtained that temperature effect on drain current is more prominent on $\langle 110 \rangle$ surface compared to $\langle 001 \rangle$ and this has been demonstrated for both with and without incorporating wave function penetration. The phenomenon has been explained from a quantum mechanical viewpoint utilizing the transmission probability of electrons from source to drain. In recent research trend, MOS device is not a mere electronic device operating alone; it may work as a part of a nanosystem and, hence, change of temperature analysis is important for control and design that substantiates the importance of the present work.

Quantum ballistic transport model

The simulation model used for this work is evolved from the nanoMOS 3.5 which simulates a planar double-gate (DG) structure (Ren et al. 1914) with non-equilibrium Green's function (NEGF) approach. For short channel devices with channel length $\leq$10 nm, carrier scattering is diminished and carrier transport becomes ballistic. So, for short channel devices, ideal ballistic transport with no carrier scattering can be considered.

Although phonon scattering effects are likely to be present in such devices, for channel length $\leq$10 nm, inelastic scattering process involves energy relaxation that helps the MOSFET to achieve ballistic current (Tsuchiya and Takagi 2008). In short channel devices, both elastic and inelastic phonon scattering can be observed. When elastic scattering occurs, channel current is degraded from ideal ballistic limit due to backscattering of electrons towards the source. But when electrons undergo inelastic emission, they lose energy and, hence, can never get back again to the source overcoming the potential barrier. These electrons can only flow towards the drain without any backscattering. As inelastic emission probability is much higher than elastic emission, the inelastic emission thus improves ballistic performance (Tsuchiya and Takagi 2008). So regardless of the presence of any phonon scattering phenomenon in short channel devices, ideal ballistic condition can be assumed due to high probability of inelastic emission.

This NEGF ballistic transport model performs self-consistent solution of 2D Poisson and Schrödinger's equations using a decoupled mode space approach. The NEGF formalism is a convenient method for evaluating the transport of electrons. For each point on the grid, a Hamiltonian matrix is formed utilizing finite difference equation between two neighboring points to compute charge density. At the boundaries in the leftmost and rightmost points, i.e., source and drain contacts, the Hamiltonian is formed with self-energy terms. The self-energy term is included to account for contact coupling of source and drain which are considered as large reservoirs of electrons (Ren et al. 1914; Venugopal et al. 2002).

In mode space approach, the solver breaks down the 2D Schrödinger's equation into two one-dimensional (1D) Schrödinger's equations along the gate confinement (z) direction and along the transport (x) direction. The Poisson's equation is first solved with the charge from an initial band profile as the estimated potential. Then for each position, x, along the channel, the Schrödinger's equation is solved to obtain a set of eigen-energies and eigenfunctions (modes) along the z direction for each subband i, given as (Ren et al. 1914; Venugopal et al. 2002):

$$-\frac{\hbar^2}{2m_z^*}\frac{\partial^2}{\partial z^2}\Psi_i(x,z) + E_C(x,z)\Psi_i(x,z) = E_i(x)\Psi_i(x,z) \quad (1)$$

where m_z^* is electron effective mass in z direction, $E_C(x, z)$ is the energy of the bottom of the conduction band and $\Psi_i(x,z)$ and $E_i(x)$ are the wave function and eigenenergy, respectively, for subband i at slice x.

The 2D electron density for a subband i at a longitudinal energy E is expressed as:

$$n_i = \frac{1}{a}\sqrt{\frac{m_y^* kT}{2\pi^3\hbar^2}}[F_{-\frac{1}{2}}(\mu_S - E)A_S - F_{-\frac{1}{2}}(\mu_D - E)A_D] \quad (2)$$

where a is grid spacing along the x direction; μ_S, μ_D are Fermi levels at source and drain, respectively; A_S, A_D are corresponding spectral density functions, $F_{-\frac{1}{2}}$ is the Fermi–Dirac integral of order $(-\frac{1}{2})$, m_y^* is electron effective mass in y direction, k is Boltzman's constant and T is the operating temperature.

The resulting spatial charge distribution from net 2D charge density obtained from all subbands in the quantum well is inserted in the Poisson equation to update a new potential profile. This process is continued until the desired convergence is achieved. Finally, the quantum ballistic current and transmission coefficient are calculated for each subband. Thus, the ballistic drain current (I_i) is readily obtained by summing up the currents from all subbands expressed as:

$$I_i = \int_0^\infty I_i(E)dE \quad (3)$$

where

$$I_i(E) = \frac{q}{\hbar^2}\sqrt{\frac{m_y^* kT}{2\pi^3}}T_i(E)[F_{-\frac{1}{2}}(\mu_S - E) - F_{-\frac{1}{2}}(\mu_D - E)]$$

where $T_i(E)$ is the transmission coefficient from source to drain and $I_i(E)$ is the subband current at longitudinal energy E of subband i. $T_i(E)$ indicates the probability of the electrons that can be transmitted through the channel overcoming the energy barrier from source to drain.

Device parameters

Transport directions of DG MOSFETs fabricated on $\langle 001\rangle$ or $\langle 110\rangle$ silicon surfaces are assumed to be [100] and [001], respectively. The source and drain doping density (N_{SD}) is 10^{20} cm^{-3} (n type) and silicon body is intrinsic. The gate work-function is 4.25 eV. Effective electron masses in different directions for different valleys in $\langle 001\rangle$ and $\langle 110\rangle$ silicon are presented in Table 1. The film thickness is 1.5 nm and both the top and bottom oxide thicknesses are 1.5 nm. The top and bottom gate lengths are 10 nm. Unless otherwise stated, the gate dielectric used here is SiO_2. The effective mass at a particular direction is presented as $m^* = m/m_o$ where m_o is the mass of an electron and m is the component of electron mass in that direction. Figure 1 shows the schematic of the device structure and Fig. 2 depicts a schematic of effect of wave function penetration in this device.

A wide range of gate voltage has been used to explore the effect of temperature and wave function penetration simultaneously on the wafer surfaces from $V_{GS} = 0$ V and

Table 1 Effective electron masses for different wafer surface orientation and transport direction

Wafer	Transport	Valley	m_x^*	m_y^*	m_z^*	Degeneracy
$\langle 001\rangle$	[100]	L	0.190	0.190	0.916	2
$\langle 001\rangle$	[100]	T_1	0.190	0.916	0.190	2
$\langle 001\rangle$	[100]	T_2	0.916	0.190	0.190	2
$\langle 110\rangle$	[001]	Δ_4	0.190	0.553	0.315	4
$\langle 110\rangle$	[001]	Δ_2	0.916	0.190	0.190	2

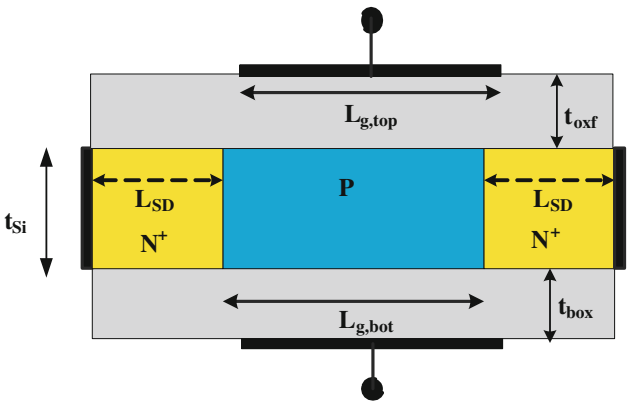

Fig. 1 Double-gate MOSFET

$V_{GS} = 0.8$ V to capture both off-state and on-state of the device. Examining the Figs. 3 and 4, the following phenomena can be inferred:

1. Wave function penetration has increased drain current I_D in both the wafer surfaces. However, the increase in current is more prominent in $\langle 110\rangle$ compared to $\langle 001\rangle$. This fact of relative higher increase in I_D due to wave function penetration in $\langle 110\rangle$ surface, is well supported by (Ashraf et al. 2009).
2. Increasing temperature has increased drain current in both the wafer surfaces. In this case, the $\langle 110\rangle$ surface is also more sensitive to temperature compared to $\langle 001\rangle$. With the same range increase in temperature (from 250 to 300, 350, 400 and 500 K), the increase in drain current is more prominent in $\langle 110\rangle$ surface. This has occurred for both circumstances incorporating with or without wave function penetration and for both on-state and off-state gate voltages as provided in Table 2.

Analysis of results

Effect of effective mass of carriers

Wave function penetration depends strongly on effective mass of semiconductor. Decrease in subband energies due to wave function penetration is higher when quantum

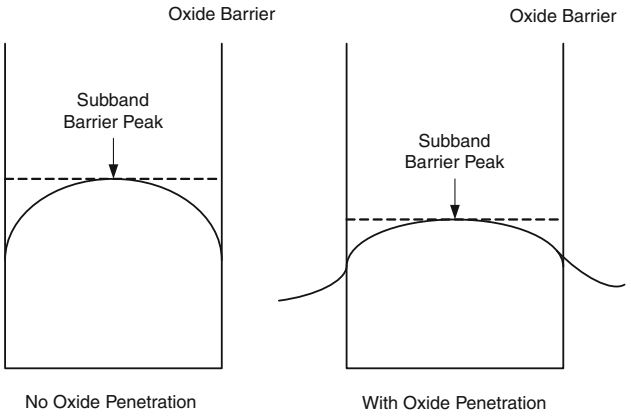

Fig. 2 Wave function and subband profile without and with penetration in oxide

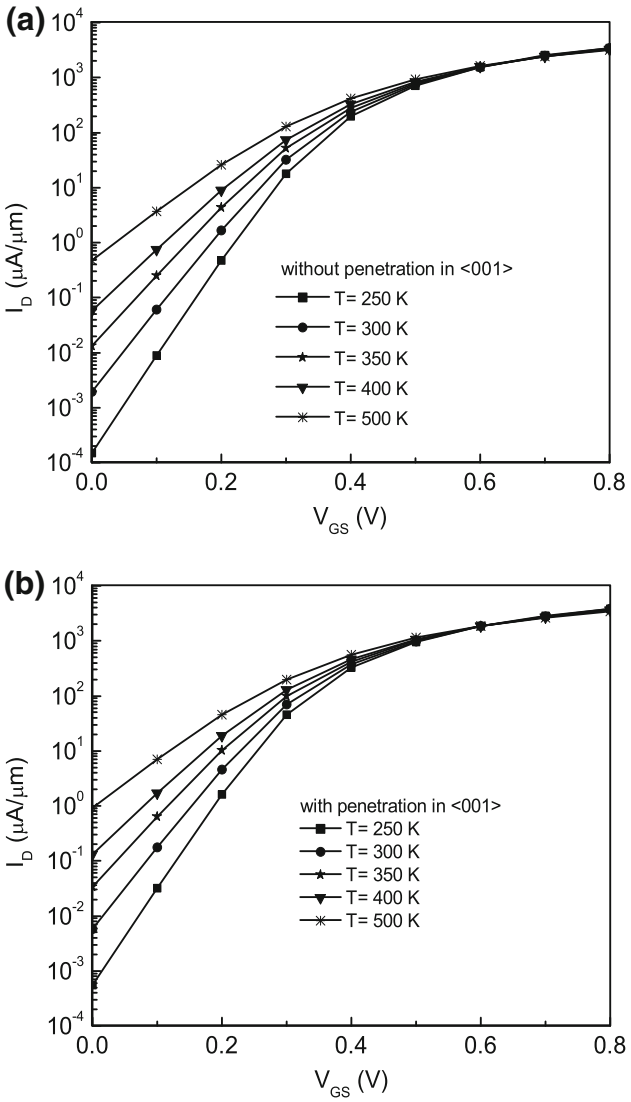

Fig. 3 Ballistic subband currents in ⟨001⟩ surface **a** without and **b** with oxide penetration

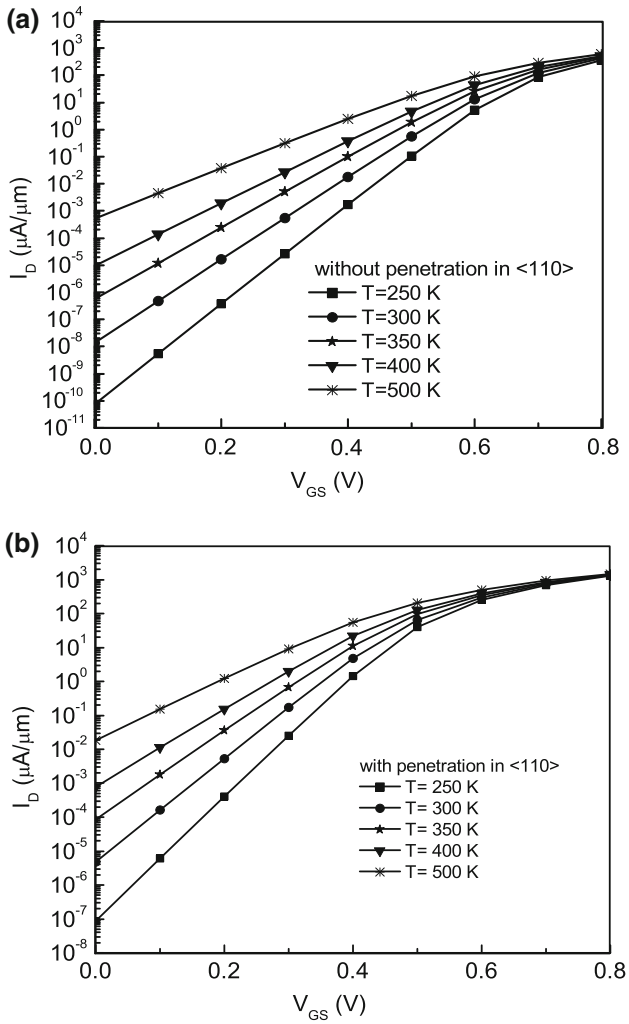

Fig. 4 Ballistic subband currents in ⟨110⟩ surface **a** without and **b** with oxide penetration

confinement of electrons is stronger. Material with low effective mass of electrons in the channels has the advantage of higher mobility and provides high wave function penetration. As depicted from Table 1, m_z^* has the same value ($0.190m_o$) in the transverse valleys T_1 and T_2 of ⟨001⟩ surface and in Δ_2 valley of ⟨110⟩ surface. Hence, wave function penetration will have similar impact of relative increase in drain current in these valleys. However, m_z^* has much lower value in Δ_4 valley of ⟨110⟩ surface compared to longitudinal valley L in ⟨001⟩. So, the effect of higher increase in overall drain current due to wave function penetration in ⟨110⟩ surface than ⟨001⟩ is dominated by the lower m_z^* in Δ_4 valley (Ashraf et al. 2009).

On the other hand, subband energy levels and energy separations are inversely related to effective mass. So if effective mass is high, subband separation narrows and subbands move closer to conduction band bottom. Thus, there exists greater probability of occupancy of electrons at

Table 2 Relative increase in I_d

Wafer	Effect	V_{GS}	$T = 250$ (I_1)	$T = 300$ (I_2)	$T = 400$ (I_3)	$T = 500$ (I_4)	I_2/I_1	I_3/I_1	I_4/I_1
Off-state current (μA/μm)									
⟨001⟩	W/O oxide	0	1.48×10^{-4}	1.94×10^{-3}	0.057	0.478	13.16	385.14	3,229.73
⟨001⟩	With oxide	0	5.49×10^{-4}	5.84×10^{-3}	0.1309	0.9276	10.64	238.43	1,689.61
⟨110⟩	W/O oxide	0	7.62×10^{-11}	1.34×10^{-8}	9.48×10^{-6}	5.26×10^{-4}	175.26	1.24×10^{5}	6.9×10^{6}
⟨110⟩	With oxide	0	8.70×10^{-8}	4.75×10^{-6}	7.83×10^{-4}	0.0182	54.54	9,000	2.09×10^{5}
On-state current (μA/μm)									
⟨001⟩	W/O oxide	0.5	711.1	754.3	843	930.7	1.06	1.19	1.31
⟨001⟩	With oxide	0.5	943.5	983.2	1,063	1,141	1.04	1.13	1.21
⟨110⟩	W/O oxide	0.5	0.1057	0.5528	4.66	17.24	5.23	44.09	163.10
⟨110⟩	With oxide	0.5	40.04	65.15	128.4	204.6	1.63	3.21	5.11

subbands compared to the lower effective mass case. Hence, drain current value is higher for materials with high effective mass which is also supported from (3).

These two impacts of effective mass are clearly supported by the results of the present work. Due to overall high effective mass in ⟨001⟩ surface, the drain current values are higher at any temperature compared to the drain currents of ⟨110⟩ surface. But due to lower effective mass, ⟨110⟩ surface gets greater impact of wave function penetration compared to ⟨001⟩ surface that can be visualized in its higher increase in drain current in Table 2.

Analysis of transmission coefficient

The effect of temperature and wave function penetration can be illustrated from the conduction band structure of silicon in the ⟨001⟩ and ⟨110⟩ surfaces. As shown in the Table 1, for ⟨001⟩, the band structure is composed of three sets of ellipsoids. The first set (L) have their longitudinal effective mass oriented along the confinement direction and give rise to unprimed subband with twofold degeneracy. The remaining two (T_1 and T_2) have their transverse effective mass oriented along the confinement direction and are primed subband with fourfold degeneracy. However, for ⟨110⟩, two sets Δ_4 and Δ_2 exist having four and two valley degeneracy, respectively. One subband for each conduction band valley is included and these subbands are independently treated in a nanoMOS simulator. This is done as in the ballistic limit; there is no scattering and mixing of electrons from different subbands (Table 3).

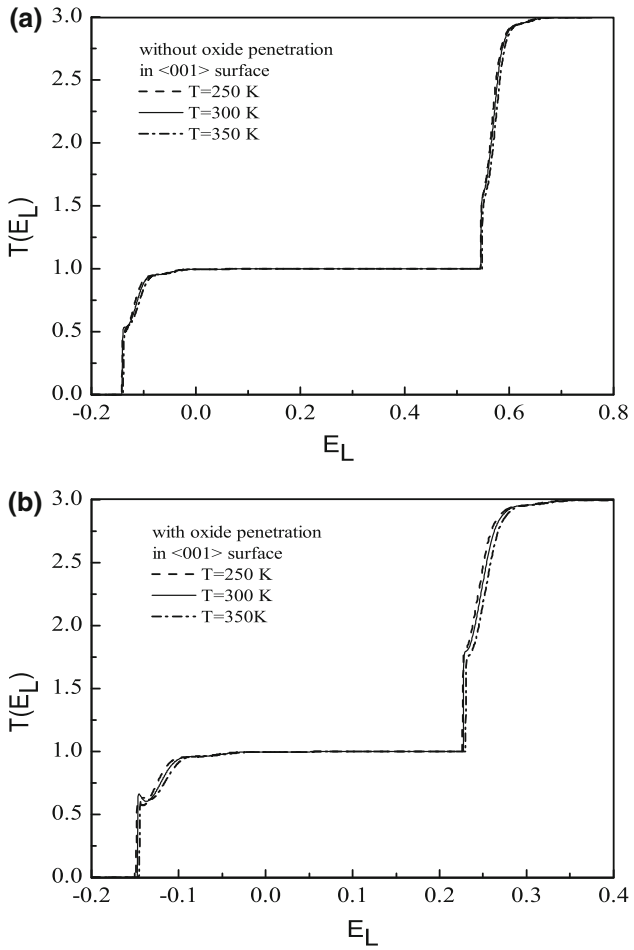

Fig. 5 Transmission coefficient in ⟨001⟩ surface **a** without and **b** with oxide penetration

Table 3 Parameters for different gate oxides

Material parameter (Robertson 2004)	Dielectric materials		
	SiO_2	Y_2O_3	ZrO_2
Dielectric constant, κ	3.9	15	25
Electron affinity (ΔE_C eV)	3.1	2.3	1.5

The source to drain transmission coefficient has been used to have a closer visualization of the wave function penetration phenomenon. The independent transmission

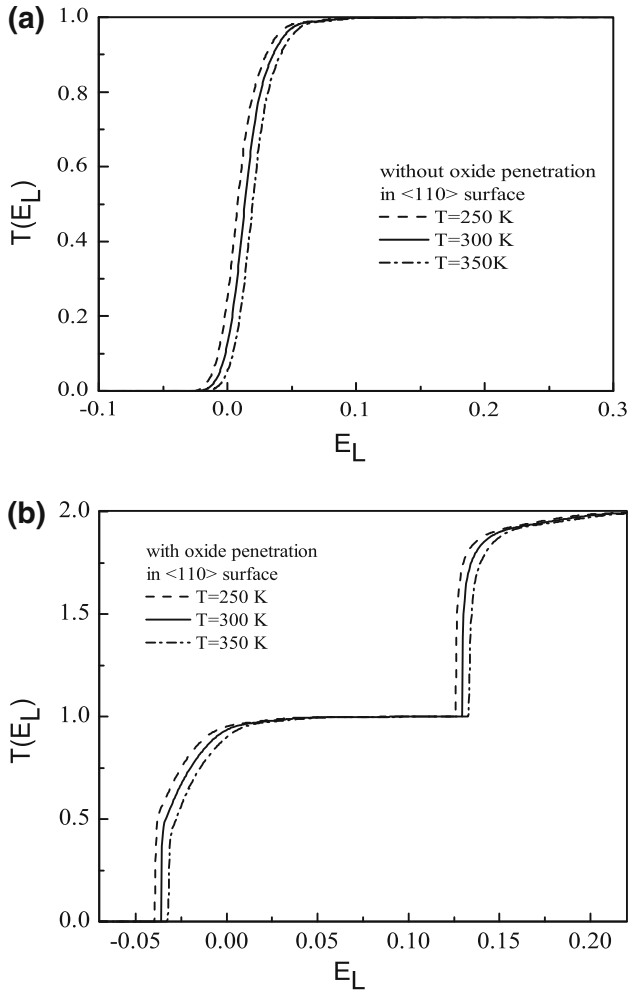

Fig. 6 Transmission coefficient in ⟨110⟩ surface **a** without and **b** with oxide penetration

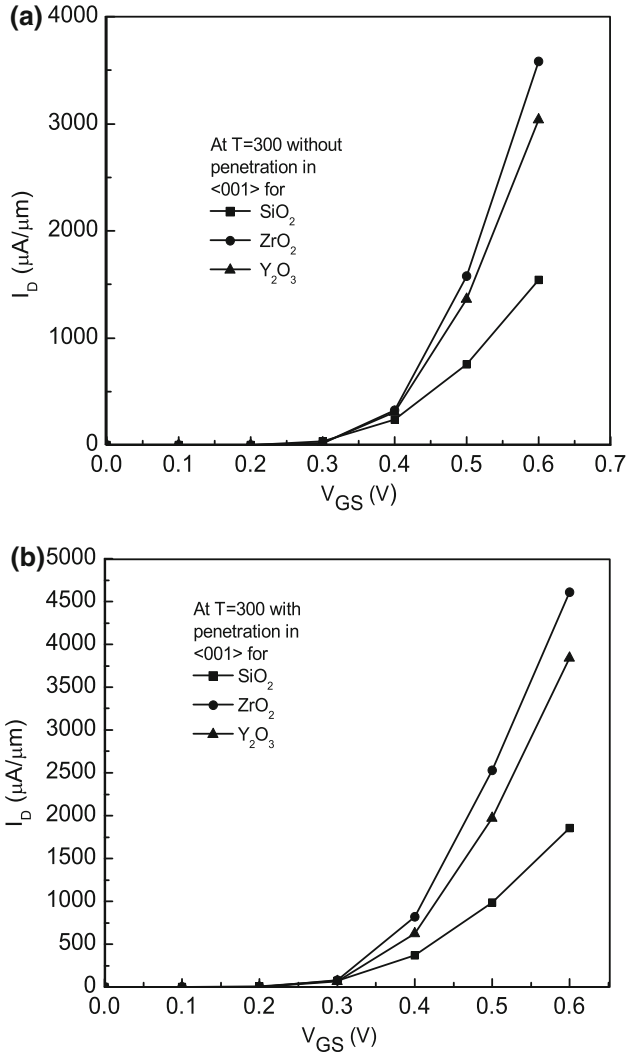

Fig. 7 Ballistic subband currents in ⟨100⟩ surface **a** without and **b** with oxide penetration for different gate oxides

coefficients of all the subbands are added to get the net transmission coefficient (T(E_L)) at each longitudinal energy (E_L). Figures 5 and 6 show the ballistic source to drain T(E_L) plotted as a function of E_L in the on-state for ⟨001⟩ and ⟨110⟩ surfaces, respectively. For the ⟨001⟩ surface, T(E_L) begins to increase below the first subband minimum, due to source to drain tunneling and rises smoothly to unity when the first subband minimum is reached. The rising of T(E_L) continues for higher energies and gradually reaches three when the electron reaches the remaining two subbands with energy degeneracy.

As visualized from Fig. 5, for the ⟨001⟩ surface, when wave function penetration occurs at a particular temperature, T(E_L) coefficient reaches quickly to 3 at lower E_L compared to without wave function penetration. This occurs as wave function penetration reduces barrier height and increases gate capacitance (Chim et al. 2003; Khan et al. 2007). Thus it induces greater amount of charge in the channel with a lower energy.

For ⟨110⟩ surface, however, besides this lower longitudinal energy phenomenon, wave function penetration has a more profound impact on the T(E_L) as it reaches to 1, i.e., only one subband of the two Δ valleys is occupied. Wave function penetration associates the reaching of another Δ subband attaining the T(E_L) to 2. This supports the greater influence of wave function penetration on ⟨110⟩ surface compared to ⟨001⟩.

Apart from this, the greater sensitiveness to temperature of ⟨110⟩ surface compared to ⟨001⟩ is also well visualized from Figs. 5 and 6. The relative increase of drain current due to increased temperature is more prominent in ⟨110⟩ surface and it can be explained from the T(E_L) curve also. The ⟨001⟩ surface has less shifting of T(E_L) with temperature change where for ⟨110⟩, this shift of T(E_L) with changing temperature can be easily visualized.

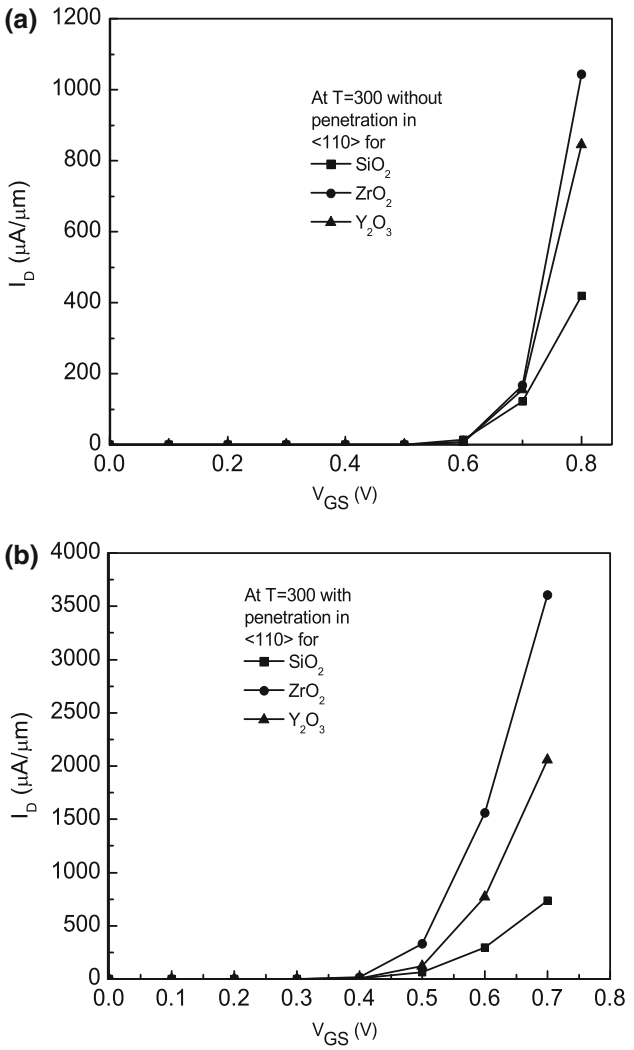

Fig. 8 Ballistic subband currents in ⟨110⟩ surface **a** without and **b** with oxide penetration for different gate oxides

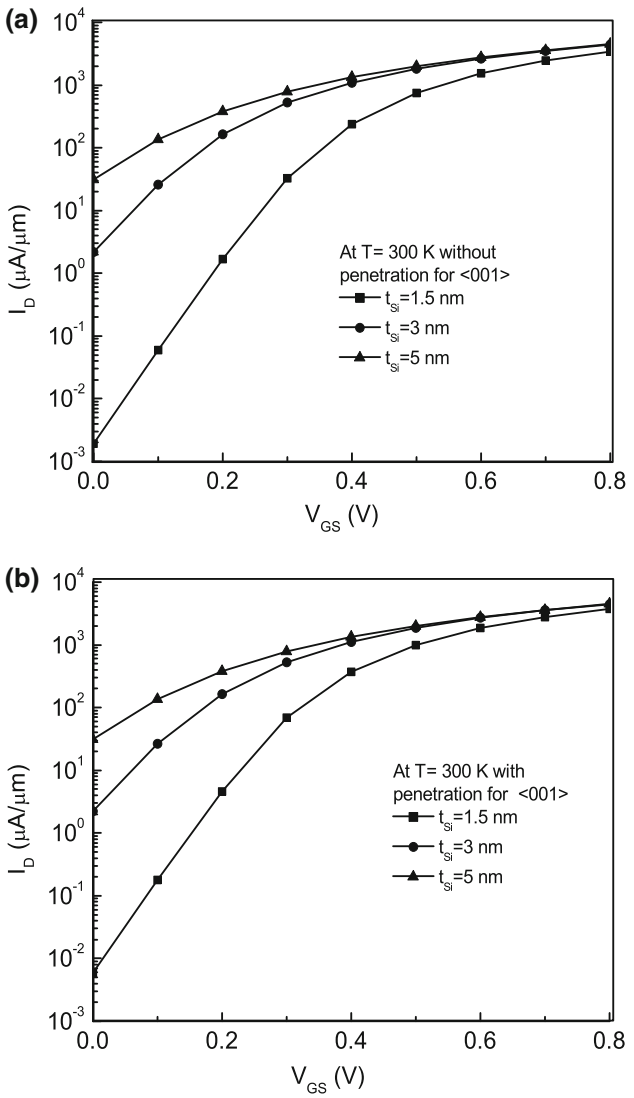

Fig. 9 Ballistic subband currents in ⟨100⟩ surface **a** without and **b** with oxide penetration for different film thicknesses

Effect of gate oxide on wave function penetration

Gate oxide materials have significant impact on wave function penetration. Oxide material sandwiching the channel has high but finite barrier and electrons are able to penetrate any finite barrier. To act as an insulator, gate oxides should have conduction band offsets with silicon of over 1 eV to minimize carrier injection into its bands. Increasing conduction band offset results in higher oxide barrier height (Robertson 2004) leading to relatively lower increase in drain current with wave function penetration. In the nanoMOS 3.5 simulator, when oxide penetration is considered, the conduction band offset is added to the potential profile while solving Schrödinger's equation. So using different oxides with different conduction band offset, the gate oxide regions can have different values of finite barrier height. Hence, relative increase in drain current due to wave function penetration is affected accordingly. These phenomena are also supported in the present work in Figs. 7 and 8. The surface ⟨110⟩ showed greater increase in drain current with wave function penetration. ZrO_2 having lowest value of conduction band offset (ΔE_C) provided the lowest oxide barrier and resulted in the highest increase in drain current compared to Y_2O_3 and SiO_2.

Effective mass of electron in oxide can also have impact on wave function penetration. But in the mode space approach used in the present work, while solving the z directed effective mass Schrödinger's equations of (1), quantization effective mass m_z^* is kept independent of (x,y). So, it is assumed $m_z^*(\text{oxide}) = m_z^*(\text{Si})$ (Svizhenko et al. 2001). As continuity of effective mass is maintained in channel and gate oxide in the nanoMOS 3.5 simulator, the effect of effective mass in oxide is ignored here.

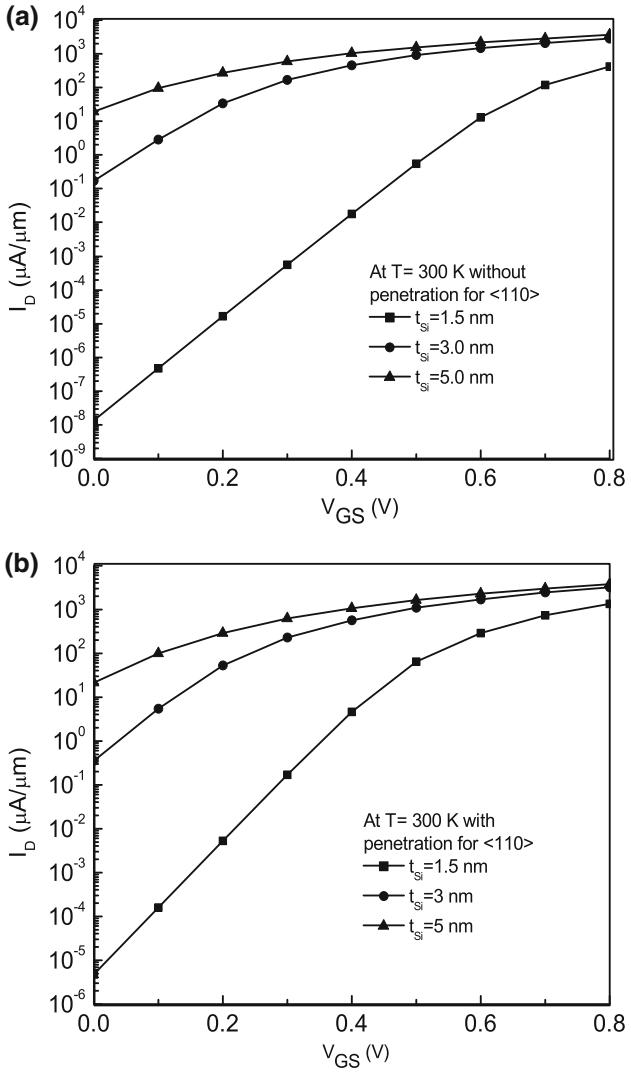

Fig. 10 Ballistic subband currents in ⟨110⟩ surface **a** without and **b** with oxide penetration for different film thicknesses

Effect of film thickness on wave function penetration

Results with thicker channels have been incorporated in Figs. 9 and 10. For thinner channel $t_{Si} = 1.5$ nm, effect of wave function penetration is more dominant compared to thicker channels. This occurs because with reduced film thickness, the distance between subband energy and conduction band increases and subband separation is also high. On the other hand, for thick films, subband separation is narrow and subbands remain closer to the conduction band. So, for thin film, when wave function penetration occurs and subband energy level is reduced, carrier concentration highly increases in these lower bands. Hence, large increase in drain current is observed. But for thick films, as subband distance and separation both are low, the effect of reducing subband energy level due to wave function penetration is not observed clearly as for thin films. Hence, thinner films exhibit greater of wave function penetration. Also in ⟨110⟩ surface, wave function penetration is affected more with channel thickness scaling compared to ⟨001⟩. This phenomenon is also supported by (Ashraf et al. 2009).

Conclusion

In this paper, the effects of temperature on the ballistic drain current of DG MOSGET have been investigated. A quantitative comparison has been presented for two different surface orientations of DG MOSFETs. Wave function penetration into gate oxide has also been considered. It has been found that both on-state and off-state currents are affected with temperature for both surface orientations. Inclusion of wave function penetration has significant impact on these currents. ⟨110⟩ surface is affected much more compared to ⟨001⟩.

Acknowledgments The authors would like to acknowledge the nanoHUB.org for their quantum transport simulator, nanoMOS 3.5.

References

Ashraf MK, Khan AI, Haque A (2009) Wave function penetration effects on ballistic drain current in double gate MOSFETs fabricated on ⟨100⟩ and ⟨110⟩ silicon surfaces. Solid State Electron 53:271

Chim WK, Zheng JX, Koh BH (2003) Modeling of charge quantization and wave function penetration effects in a metal-oxidesemiconductor system with ultrathin gate oxide. J Appl Phys 94(8):5273

Farzana E, Chowdhury S, Ahmed R, Khan MZR (2012) Performance analysis of nanoscale double gate MOSFETs with high-κ gate stack. Appl Mech Mater 110−116:1892. doi:10.4028/www.scientific.net/AMM.110-116.1892

Haque A, Kauser MZ (2003) A comparison of wave-function penetration effects on gate capacitance in deep submicron n- and p-MOSFETs. IEEE Trans Electron Devices 49(9):1580

Iwai H (2009) Roadmap for 22 nm and beyond. Microelectron Eng 86(7–9):1520

Kauser MZ, Hasan MS, Haque A (2002) Effects of wave function penetration into the gate-oxide on self-consistent modeling of scaled MOSFETs. IEEE Trans Electron Devices 49(4):693

Khan AI, Ashraf MK, Khoshru QDM (2007) Effects of wave function penetration on gate capacitance modeling of nanoscale double gate MOSFETs. Electron Devices Solid State Circuits EDSSC, pp 137–140

Monaghan S, Hurley P, Cherkaoui K, Negara M, Schenk A (2009) Determination of electron effective mass and electron affinity in HfO_2 using MOS and MOSFET structures. Solid State Electron 53(4):438

Ren Z, Venugopal R, Goasguen S, Datta S, Lundstrom MS (2003) nanoMOS 2.5: a two-dimensional simulator for quantum

transport in double-gate MOSFETs. IEEE Trans Electron Devices 50(9):1914

Robertson J (2004) High dielectric constant oxides. Eur Phys J Appl Phys 28:265

S.I. Association. International Technology Roadmap for Semiconductors (2009). http://www.itrs.net/links/2009ITRS/Home2009.htm

Svizhenko A, Anantram MP, Govindan TR, Biegel B, Venugopal R (2001) Two-dimensional quantum mechanical modeling of nanotransistors. J Appl Phys 91(4):2343

Tsuchiya H, Takagi S (2008) Influence of elastic and inelastic phonon scattering on the drive current of quasi-ballistic MOSFETs. IEEE Trans Electron Devices 55(9):2397

Tsutsui G, Hiramoto T (2006) Mobility and threshold-voltage comparison between ⟨110⟩- and ⟨100⟩-oriented ultrathin-body silicon MOSFETs. IEEE Trans Electron Devices 53(10):2582

Venugopal R, Ren Z, Datta S, Lundstrom MS (2002) Simulating quantum transport in nanoscale MOSFETs: real versus mode space approaches. D Jovanovic J Appl Phys 92(7):3730

Yunus M, Haque A (2003) Wave function penetration effects on current voltage characteristics of ballistic metal-oxide-semiconductor transistors. J Appl Phys 93(1):600